DOI 10.1007/s11182-015-0571-0

Russian Physics Journal, Vol. 58, No. 6, October, 2015 (Russian Original No. 6, June, 2015)

MICROSTRUCTURE AND MECHANICAL PROPERTIES OF THE Ti–45Al–5Fe INTERMETALLIC ALLOY

T. I. Nazarova, V. M. Imayev, and R. M. Imayev

UDC 669.295

Microstructure including changes in the phase composition and mechanical compression properties of the Ti–45Al–5Fe *(at.%) intermetallic alloy manufactured by casting and subjected to homogenization annealing are investigated as functions of the temperature. The initial alloy has a homogeneous predominantly lamellar structure with relatively small size of colonies of three intermetallic phases:* $\gamma(TiAl)$*,* $\tau_2(Al_2FeTi)$*, and* $\alpha_2(Ti_3Al)$ *in the approximate volume ratio 75:20:5. Compression tests have revealed the enhanced strength at room temperature and the improved hot workability at 800°C compared to those of TNM alloys of last generation.*

Keywords: gamma titanium aluminides, microstructure, mechanical properties.

INTRODUCTION

Light intermetallic alloys based on $\gamma(TiAl) + \alpha_2(Ti_3Al)$ phases are treated as a partial replacement for creep resistant nickel based superalloys and steels in new generation gas turbine engines and modern ground-based energy conversion systems that will significantly improve their power efficiency. Blades, disks, parts of nozzles, and other elements can be manufactured from these alloys. At present, $\gamma(TiAl) + \alpha_2(Ti_3Al)$ alloys are used as a structural material for the low-pressure turbine blades in the last two stages of the gas turbine engine developed for Boeing 787 and Boeing 747-8 aeroplanes [1]. Nevertheless, materials science of the intermetallic $\gamma(TiAl) + \alpha_2(Ti_3Al)$ alloys continues to be developed in directions of developing new alloys and casting technologies, novel hot working and heat treatment processing, methods optimizing microstructural state and developing technologies based on methods of powder metallurgy [2–7]. So, $\gamma(TiAl) + \alpha_2(Ti_3Al)$ alloys of last generation (Ti Nb-containing (TNB) alloys and Ti alloys with Nb and Mo additions (TNM alloys)) possess the specific strength and creep and oxidation resistances higher than those of $\gamma(TiAl) + \alpha_2(Ti_3Al)$ alloys of preceding generation and have quite acceptable ductility at room temperature (around 2–3.5% of elongation) after hot deformation processing [2, 4, 5, 7]. At the same time, low casting properties, high labor consumption of hot working and machining, low ductility and crack resistance of the $\gamma(TiAl) + \alpha_2(Ti_3Al)$ alloys at temperatures below the brittle-ductile transition temperature ($T \approx 800$°C), in particular, in the cast state still hinder the application of these materials.

The factor sufficiently increasing the brittleness of the cast $\gamma(TiAl) + \alpha_2(Ti_3Al)$ alloys is the presence of the lamellar $\alpha_2(Ti_3Al)$ phase prone to partial disordering and totally brittle at room temperature [8, 9]. The present work is aimed at the substitution of the $\alpha_2(Ti_3Al)$ phase ($D0_{19}$ superlattice) by another $\tau_2(Al_2FeTi)$ intermetallic phase ($D8_a$ superlattice) and at the transition from the lamellar microstructure with high density of coherent and half-coherent boundaries, considered to be most preferable for the $\gamma(TiAl) + \alpha_2(Ti_3Al)$ alloys, to the matrix microstructure hardened by finely dispersed precipitations.

The Ti–45Al–5Fe (at.%) alloy chosen based on the Al–Fe–Ti ternary phase diagram [10, 11], according to which the alloy should consist of the intermetallic $\gamma(TiAl)$ and $\tau_2(Al_2FeTi)$ phases at room temperature, is studied in the

Institute for Metals Superplasticity Problems of the Russian Academy of Sciences, Ufa, Russia; e-mail: nazarova.ti@mail.ru; vimayev@mail.ru; renat_imayev@mail.ru. Translated from Izvestiya Vysshikh Uchebnykh Zavedenii, Fizika, No. 6, pp. 52–56, June, 2015. Original article submitted March 6, 2015.

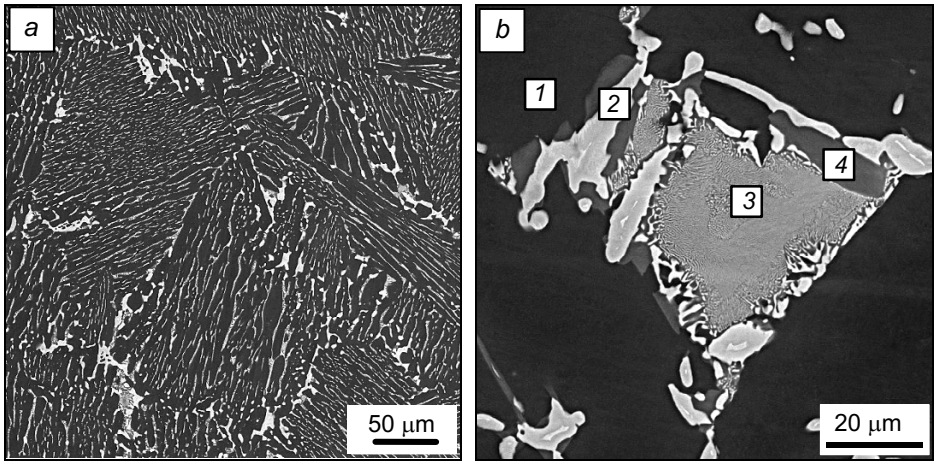

Fig. 1. BSE images of the Ti–45Al–5Fe (at. %) alloy after HA obtained at different magnifications.

present work. The phase composition of the alloy is investigated as a function of the quenching temperature, and mechanical compression tests are performed. Results of the mechanical tests are compared with the properties of the TNM alloys [4, 12] – γ(TiAl) + α_2(Ti_3Al) alloys of last generation.

MATERIAL AND EXPERIMENTAL PROCEDURE

The Ti–45Al–5Fe (at.%) alloy was used as the initial material. The ingot of the examined alloy with a weight of about 30 g was manufactured by argon-arc melting in a laboratory facility. To achieve high chemical homogeneity, the ingot was remelted at least 7 times. Microstructural investigations were performed using a Tescan Mira3 scanning electron microscope operating in the backscattered electron (BSE) mode. An x-ray diffraction analysis was performed using CoK_α radiation. ATS furnaces with kanthal ($MoSi_2$) heaters were used for heat treatment. Homogenization annealing (HA) was performed at T = 1100°C (τ = 3 h) followed by furnace cooling. Experiments on water quenching were performed after annealing at temperatures T = 800–1300°C (τ = 1 h). The quenched specimens were investigated by the methods of x-ray diffraction and electron microscopy. Mechanical compression tests were performed in air at T = 20 and 800°C with initial strain rate $\varepsilon' \approx 10^{-3}$ s^{-1}. The specimens had sizes 5 × 5 × 8 mm^3. Two specimens per point were tested.

RESULTS AND DISCUSSION

The microstructure of the cast alloy subjected to HA is shown in Fig. 1. The alloy microstructure was homogeneous and had basically lamellar morphology. The average size of colonies was about D = 150 μm (Fig. 1*a*), and the globular grain size at the boundaries of the colonies was d = 10–40 μm. Thus, the microstructure obtained was much finer than that typical for the Ti–(45–47)Al binary alloys [3]. It seems likely that the relatively fine-grained cast structure was caused by the phase transformations that occurred in the alloy during cooling after solidification.

Results of the x-ray diffraction analysis of the Ti–45Al–5Fe alloy subjected to HA and quenching experiments at the indicated temperatures are shown in Fig. 2. Peaks of three phases – γ(TiAl), τ_2(Al_2FeTi), and α_2(Ti_3Al) – are presented in the x-ray diffraction pattern of the initial state after HA. SEM observations revealed four microstructural constituents (Fig. 1*b*) that differed by their contrasts; their chemical composition is given in Table 1. Dark region *1* corresponds to the chemical composition of the γ(TiAl) phase [10]. Light region *2* is enriched by iron (up to 21 at.%) and can be identified as the τ_2(Al_2FeTi) phase [10, 11]. It seems likely that region *3* is eutectic one consisting of the

TABLE 1. Results of EDX Analysis of the Regions Shown in Fig. 1*b*

Region	Composition, at.%			
	Al	Ti	Fe	Phase
1	48.23 ± 1	49.53 ± 1	2.24 ± 0.12	γ(TiAl)
2	38.92 ± 1	39.95 ± 1	21.14 ± 1	$\tau_2(Al_2FeTi)$
3	33.65 ± 1	58.33 ± 1	8.03 ± 0.5	$\tau_2(Al_2FeTi)+\alpha_2(Ti_3Al)$
4	35.94 ± 1	62.50 ± 1	1.75 ± 0.2	$\alpha_2(Ti_3Al)$

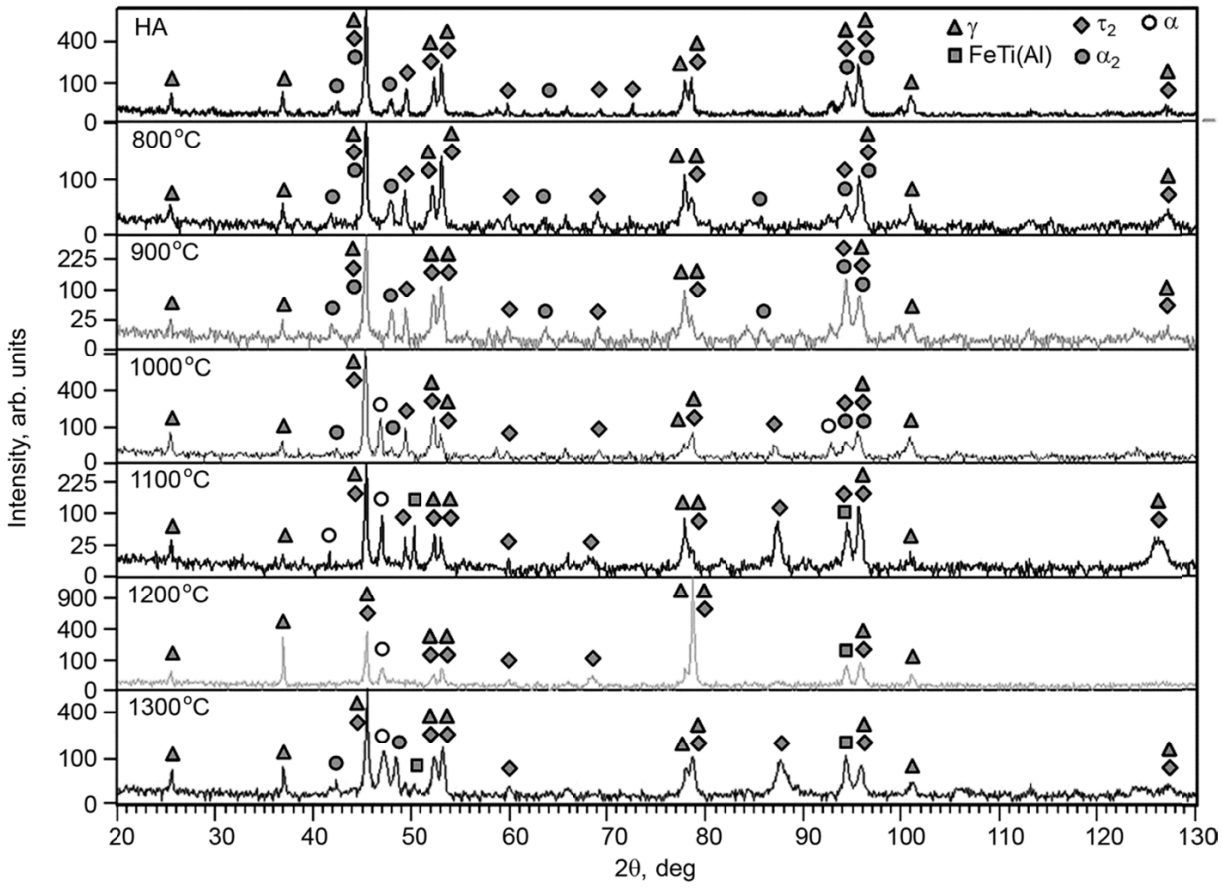

Fig. 2. X-ray diffraction patterns of the cast Ti–45Al–5Fe (at.%) alloy subjected to HA and annealing at the indicated temperatures (in the interval T = 800–1300°C) followed by water quenching.

mixture of the $\tau_2(Al_2FeTi)$ and $\alpha_2(Ti_3Al)$ phases. Grey region *4* is iron- and aluminum-depleted; its composition coincides with the $\alpha_2(Ti_3Al)$ phase [10, 13]. The combined x-ray diffraction, microstructural, and energy dispersive analyses allowed the phase composition of the alloy and the approximate quantitative ratio of phases to be determined as 75 vol.% γ(TiAl), 20% $\tau_2(Al_2FeTi)$, and 5 vol.% $\alpha_2(Ti_3Al)$ (see Figs. 1 and 2 and Table 1).

After quenching from temperatures T = 800–900°C, the alloy in the initial state contained three phases – γ(TiAl), $\tau_2(Al_2FeTi)$, and $\alpha_2(Ti_3Al)$ – in good agreement with the experimental data presented in [10] (Figs. 2 and 3*a*). We note that according to the calculated Al–Fe–Ti ternary phase diagram, the alloy should contain two phases – γ(TiAl) and $\tau_2(Al_2FeTi)$ at T = 800°C [11].

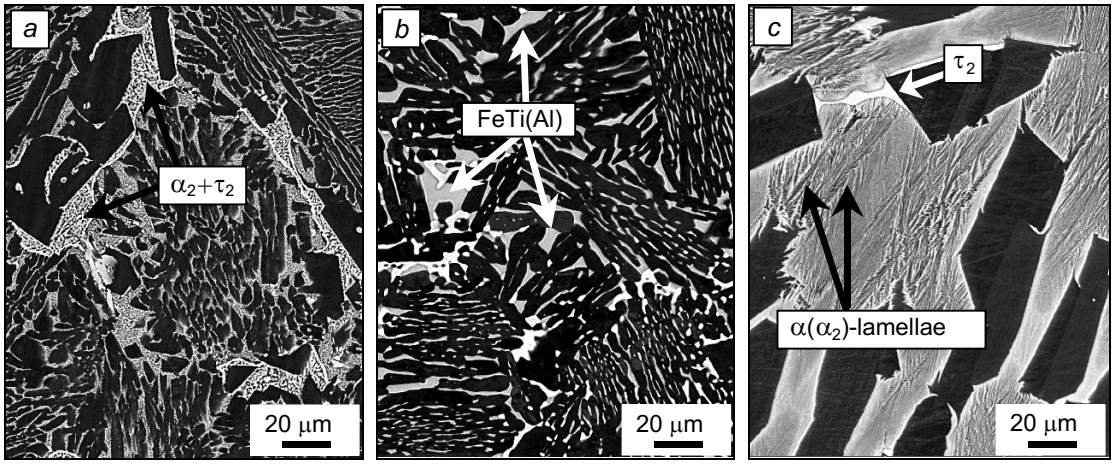

Fig. 3. BSE image of the Ti–45Al–5Fe (at.%) alloy subjected to water quenching from temperatures $T = 900$ (*a*), 1100 (*b*), and 1300°C (*c*).

Quenching from the temperature $T = 1000$°C led to the occurrence of peaks of the disordered α-phase in the x-ray diffraction pattern with retention of peaks of the α_2-phase. The γ(TiAl) and $\tau_2(Al_2FeTi)$ phases remained the main ones.

It seems likely that after quenching from the temperature $T = 1100$°C, the α_2-phase is completely (or almost completely) disordered, since no peaks of the α_2-phase are observed (Fig. 2). The basic phases – γ(TiAl) and $\tau_2(Al_2FeTi)$ – retain their presence in the alloy. Moreover, the peaks of the FeTi(Al) pseudobinary phase of light grey color are observed in the electron microscopic image (Fig. 3*b*). It can be seen that when the quenching temperature increased from 900 to 1100°C (Fig. 3*a* and *b*), the mixture of the α_2 and τ_2 phases localized along the boundaries of the $(\gamma + \tau_2)$ colonies undergoes the phase transformation via one of three possible reactions with participation of the γ(TiAl) phase of the form $\alpha_2 + \tau_2 \Rightarrow \gamma + \text{FeTi(Al)}$ [14].

After quenching from the temperature $T = 1200$°C, the peaks of four phases – γ, τ_2, α, and FeTi(Al) – were observed in the x-ray diffraction pattern. The EDX analysis demonstrated that the FeTi(Al) phase was strongly depleted by iron, its content was close to that of the mixture of the $\tau_2(Al_2FeTi) + \alpha_2(Ti_3Al)$ phases (Table 1), and on average, corresponded to 35 at.% Al, 55 at.% Ti, and 9 at.% Fe. This is in agreement with the results presented in [13, 14], where it was demonstrated that 90% of iron in the FeTi(Al) pseudo-binary phase could be substituted by aluminum and titanium, i.e., the iron content in this phase could be decreased down to 5 at.%.

Quenching from the temperature $T = 1300$°C, in comparison with $T = 1200$°C, led to an increase in the integral intensity of the peaks of the disordered α-phase and ordered α_2-phase (Fig. 2). It seems likely that at high temperatures, the FeTi(Al) pseudo-binary phase decomposes into τ_2 (light interlayers) and $\alpha(\alpha_2)$ (lamellae) according to the reaction $\gamma + \text{FeTi(Al)} \Rightarrow \tau_2 + \alpha(\alpha_2)$ (Fig. 3*c*). We note that the possibility of such phase transformation in the Al–Fe–Ti alloy was demonstrated in [14]. In [13] the formation of the α_2-phase lamellae in the Ti–48.5Al–2Fe alloy was also observed after quenching from $T = 1300$°C.

Hence, based on the results of the x-ray diffraction, microstructural, and EDX analyses of the alloy specimens subjected to annealing and subsequent water quenching, the sequence of the phase regions with temperature increasing in the interval $T = 800$–1300°C can be represented as follows: $\gamma + \tau_2 + \alpha_2 \Rightarrow \gamma + \tau_2 + \alpha(\alpha_2) \Rightarrow \gamma + \tau_2 + \alpha + \text{FeTi(Al)} \Rightarrow \gamma + \tau_2 + \alpha(\alpha_2) + \text{FeTi(Al)}$ (see Figs. 2 and 3 and Tables 1 and 2).

Compression tests were performed for the alloy subjected to HA (Table 3). A comparison of the mechanical properties obtained with the properties of the $\gamma(TiAl) + \alpha_2(Ti_3Al)$ alloys of last generation [4, 12] demonstrated that the Ti–45Al–5Fe alloy had the increased strength at room temperature with retention of similar ductility. The material was deformed at increased temperature ($T = 800$°C) by 70% without fracture at lower values of the yield strength, which testified to the improved hot workability of the Ti–45Al–5Fe alloy. It should be noted that among the advantages of the examined alloy are: 1) the absence of necessity of boron addition to refine the initial cast structure and 2) the

TABLE 2. Phase Composition of the Ti–45Al–5Fe (at.%) Alloy Depending on the Quenching Temperature

Quenching temperature, °C	Phase composition
800	$\gamma + \tau_2 + \alpha_2$
900	$\gamma + \tau_2 + \alpha_2$
1000	$\gamma + \tau_2 + \alpha(\alpha_2)$
1100	$\gamma + \tau_2 + \alpha$ + FeTi(Al)
1200	$\gamma + \tau_2 + \alpha$ + FeTi(Al)
1300	$\gamma + \tau_2 + \alpha(\alpha_2)$ + FeTi(Al)

TABLE 3. Mechanical Compression Properties of the Ti–5Al–5Fe (at.%) Alloy Compared with the γ(TiAl) + α_2(Ti_3Al) Alloys of Last Generation (TNM Alloys)

Alloy, at.%	20°C			800°C	
	$\sigma_{1.25}$, MPa	σ_{US}, MPa	ε,%	$\sigma_{1.25}$, MPa	ε,%
Ti–45Al–5Fe	1018	2010	15	648	70*
Ti–45Al–6(Nb, Mo)–0.2B	928	1656	16	688	70**
Ti–43Al–6(Nb, Mo)–0.2B	1388	1899	8.4	1078	70**

Notes: *The material deformed without fracture; **cracks were observed on the side surface of the deformed specimens.

substitution of the brittle α_2(Ti_3Al) phase by the intermetallic τ_2(Al_2FeTi) phase with insignificant content of the globular α_2(Ti_3Al) phase. At the same time, further investigations of the mechanical behavior of the material are required.

CONCLUSIONS

Our investigations have shown that a homogeneous predominantly lamellar microstructure with the average size of colonies D = 150 μm is formed in the initial cast Ti–45Al–5Fe (at.%) alloy after HA. The phase composition of the alloy involves the γ(TiAl), τ_2(Al_2FeTi), and α_2(Ti_3Al) phases in the approximate volume ratio 75:20:5.

When the temperature increased in the interval T = 800–1300°C, the following sequence of phase regions was established: $\gamma + \tau_2 + \alpha_2 \Rightarrow \gamma + \tau_2 + \alpha(\alpha_2) \Rightarrow \gamma + \tau_2 + \alpha$ + FeTi(Al) $\Rightarrow \gamma + \tau_2 + \alpha(\alpha_2)$ + FeTi(Al).

The mechanical compression properties of the Ti–45Al–5Fe alloy after homogenization annealing were investigated. The comparison of the alloy properties with those of the TNM alloys of last generation demonstrated that the presence of the τ_2(Al_2FeTi) phase instead of the α_2(Ti_3Al) phase promoted the achievement of high strength of the cast material at T = 20°C and improved the hot workability at T = 800°C.

REFERENCES

1. B. P. Bewlay, in: European Symposium on Superalloys and their Applications, Wildbad Kreuth (2010), pp. 25–28.
2. F. Appel, J. D. H. Paul, and M. Oehring, Science and Technology, WILEY-VCH Verlag GmbH & Co. KGaA, Weinheim (2011).
3. R. Imayev, V. Imayev, M. Oehring, and F. Appel, Intermetallics, **15**, 451–460 (2007).
4. H. Clemens and S. Mayer, Adv. Eng. Mater., **15**, 191–215 (2013).
5. V. Imayev, T. Oleneva, R. Imayev, *et al*., Intermetallics, **26**, 91–97 (2012).
6. J. Aguilar, A. Schievenbusch, and O. Kaettlitz, Intermetallics, **19**, 757–761 (2011).

7. V. M. Imayev, R. M. Imayev, and T. I. Oleneva, Pis'ma Mater., **1**, No. 1, 25–31 (2011).
8. R. M. Imayev, N. K. Gabdullin, G. A. Salishchev, *et al*., Acta Mater., **47**, 1809–1821 (1999).
9. R. N. Eshchenko, O. A. Elkina, A. M. Patselov, and V. P. Pilyugin, Phys. Metals Metallogr., **102**, 611–618 (2006).
10. M. Palm, A. Gorzel, D. Letzig, *et al*., Structural Intermetallics, M. V. Nathal, R. Darolia, C. T. Liu, *et al*. eds., TMS Publications Home, Warrendale (1997).
11. V. Raghavan, J. Phase Equilibria, **23**, 367–374 (2002).
12. V. M. Imayev, T. G. Khismatullin, and R. M. Imayev, Phys. Met. Metallogr.+, **109**, No. 4, 402–410 (2010).
13. L. Levin, A. Tokar, M. Talianker, and E. Evangelista, Intermetallics, **7**, 1317–1322 (1999).
14. M. Palm, G. Inden, and N. Thomas, J. Phase Equilibria, **16**, 209–222 (1995).